Molecular vibrations-induced quantum beats in two-dimensional electronic spectroscopy

ARTICLE *in* THE JOURNAL OF CHEMICAL PHYSICS · JULY 2012

Impact Factor: 2.95 · DOI: 10.1063/1.4737843 · Source: PubMed

3 AUTHORS, INCLUDING:

Vytautas Butkus
Vilnius University
25 PUBLICATIONS **237** CITATIONS
SEE PROFILE

Darius Abramavicius
Vilnius University
118 PUBLICATIONS **2,052** CITATIONS
SEE PROFILE

Molecular vibrations-induced quantum beats in two-dimensional electronic spectroscopy

Vytautas Butkus,[1,2] Leonas Valkunas,[1,2] and Darius Abramavicius[1,3,a)]

[1)] *Department of Theoretical Physics, Faculty of Physics, Vilnius University, Sauletekio 9-III, 10222 Vilnius, Lithuania*

[2)] *Center for Physical Sciences and Technology, Gostauto 9, 01108 Vilnius, Lithuania*

[3)] *State Key Laboratory of Supramolecular Complexes, Jilin University, 2699 Qianjin Street, Changchun 130012, PR China*

Quantum beats in nonlinear spectroscopy of molecular aggregates are often attributed to electronic phenomena of excitonic systems, while nuclear degrees of freedom are commonly included into models as overdamped oscillations of bath constituents responsible for dephasing. However, molecular systems are coupled to various high-frequency molecular vibrations, which can cause the spectral beats hardly distinguishable from those created by purely electronic coherences. Models containing damped, undamped and overdamped vibrational modes coupled to an electronic molecular transition are discussed in this paper in context of linear absorption and two-dimensional electronic spectroscopy. Analysis of different types of bath models demonstrates how do vibrations map onto two-dimensional spectra and how the damping strength of the coherent vibrational modes can be resolved from spectroscopic signals.

I. INTRODUCTION

Various ultrafast spectroscopy techniques are capable of probing molecular dynamics on timescales of nuclear motion and spectroscopic signals usually reveal effects caused by the coherent exciton dynamics, energy transfer, vibrational motions, etc. perceptible even for simple systems[1–5]. For example, coherent quantum beats obtained at broadband excitation conditions are displayed in spectra of small molecular complexes[6–8], thus, reflecting an interplay between the absorbed energy transfer and relaxation.

The two-dimensional (2D) electronic spectroscopy (ES) displays highly resolved decoherence dynamics in molecular aggregates induced by the system-bath interaction. Problem of assignment of the detected slowly-decaying spectral beats to either electronic coherences[3,9–13] or molecular vibrations[14,15] is under intense discussions up to now. However, it is still disputed whether such detachment is feasible at all.

Molecules and their environment are characterized by a wide variety of high-frequency vibrational modes, some of them strongly-coupled to the electronic excitations. Unambiguous experimental evidences that the high-frequency vibrational wavepacket motion causes the spectral beats in 2D spectra were reported only recently[16–18]. However, it is not yet clearly established how these vibrational resonances map onto 2D spectra and how the excited vibrational wavepacket evolution affects the spectral dynamics.

Systems where the high-frequency vibrations are mixed with electronic transitions are currently of a special interest. Great efforts are made to effectively and universally identify the underlying mechanisms[17–20]. Analysis of rephasing and nonrephasing signals of the 2D ES separately could help solving this issue in some cases, but usually the strong spectral congestion leaves ambiguity of the result due to the overlap of many oscillating features. In case when the limited-bandwidth laser pulses cannot cover the whole absorption spectrum even if the vibrational features are well-resolved, the intramolecular vibrations can still be evaluated by analyzing the phase relationships of beating patterns in the rephasing and nonrephasing signals, peak ellipticity or rotation of the nodal line of the imaginary part of the total 2D spectrum[4,19,21]. However, vibrational coherences can be created in the electronic ground state manifold resulting in beats of both diagonal and off-diagonal peaks, thus making the whole time-resolved dynamics even more entangled[19,21].

Non-decaying vibrations-related quantum beats on top of the vertical electronic transitions are obtained in simulated time-resolved spectra when molecular vibrations are included as coherent harmonic modes of the bath coupled to the system[4,22,23]. This problem sometimes is formulated in pure quantum mechanical terminology by using so-called polaron transformation[24,25]. Such treatment is exact when non-interacting molecules are considered; however, in molecular aggregates vibrations are coupled to the electronic degrees of freedom in a non-trivial way. More sophisticated theoretical methods, for example, hierarchical equations of motion or time-dependent density matrix renormalization group technique, might resolve the dynamics of such mixed vibronic systems[26–28]. As the vibrational coherence decay rate is usually smaller compared to those of the electronic coherences, this might also trigger the reconsideration of the nature of long-lived coherences observed in many systems.

In this paper, we theoretically analyze the influence of high-frequency damped vibrational motion of molecules on the spectroscopic observables and make comparison

[a)] Electronic mail: darius.abramavicius@ff.vu.lt

with the undamped description. In the microscopic model such treatment translates into a more sophisticated expression of bath spectral density function. General bath damping mechanisms are also the problem under consideration; the model of a quantum overdamped bath is introduced and its influence upon the lineshape formation in the linear absorption and 2D spectrum is discussed. Strongly-overlapping spectra of simple electronic and vibrational systems are examined in the context of various bath models.

II. GENERIC MOLECULAR COMPLEXES

Electric fields interacting with molecular systems can affect various system degrees of freedom ranging from electronic high-energy states to low-frequency molecular vibrations. It is natural to simplify the description by taking into consideration only the most relevant types of dynamics. One of the main simplification is achieved by neglecting the non-resonant transitions with respect to the optical field under consideration: in the case of the resonant excitation with the optical laser field a molecule is described as a system consisting of two electronic energy levels, while a supramolecular complex – as an aggregate of coupled two-level electronic systems. Another standard assumption when describing electronic quantum levels of a molecule is the separation of electronic and nuclear degrees of freedom (the Born-Oppenheimer approximation). It is assumed that the electronic wavefunction rigorously follows the nuclear configuration and the energies of electronic levels become parametric functions of nuclear degrees of freedom. The equilibrium nuclear configuration which is usually different for each electronic quantum state is defined as the energy minimum with respect to the nuclei[29,30].

A. Absorption of an isolated molecule

Using the assumptions made above, electronic excitations in molecules are approximated as the Franck-Condon transitions. It is considered that the (slow) nuclear degrees of freedom remain frozen during the electronic transition and the fixed molecular nuclear configuration adjusted to the ground electronic state emerges in non-equilibrium conditions with respect to the new electronic state. As the electronic potential energy surface is assumed to be parabolic depending on the nuclear displacement in the vicinity of the equilibrium, a displaced (harmonic) oscillator model can be used in the description of the electronic transition (Fig. 1). In one dimension the electronic potential of the ground state is $V_{\rm g}(q) = \hbar\omega_0 q^2/2$ and the displaced electronic excited state is described by the potential $V_{\rm e}(q) = \omega_{\rm eg} + \hbar\omega_0(q-d)^2/2$. Here ω_0 is the vibrational frequency, $\omega_{\rm eg}$ is the energy gap between the minima of two potentials and d is a dimensionless displacement parameter determining the strength of the electron coupling with molecular vibrations. The Huang-Rhys factor $s = \frac{1}{2}d^2$ is widely used to qualify the coupling strength.

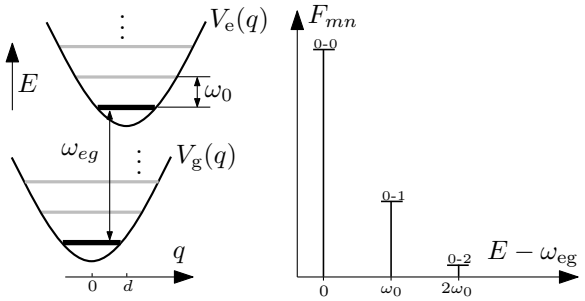

Fig. 1. Model system of displaced harmonic oscillators and Franck-Condon overlap factors for the corresponding $m-n$ transitions.

Quantum mechanical problem of the isolated harmonic potentials has exact solutions. They constitute an infinite set of wavefunctions ψ_m with quantum number $m = 0\ldots\infty$ and corresponding energies $E_m = \hbar\omega_0(m+1/2)$ with respect to the bottom of the corresponding potential surface. Transitions between the sub-states of the electronic ground state and the ones of the electronic excited state determine the vibronic progression in the absorption spectrum (Fig. 1). The intensity of each vibronic peak is scaled by the overlap of vibrational wavefunctions – the Franck-Condon overlap – in the ground and excited state potentials. Following these assumptions the absorption spectrum of a single isolated Franck-Condon molecule can be given by

$$\kappa_{\rm abs}^{\rm FC}(\omega) \propto \omega \sum_{m,n=0}^{\infty} {\rm e}^{-\frac{m\omega_0}{k_{\rm B}T}} |F_{mn}|^2 \times {\rm Re}\int_0^{\infty} {\rm d}t {\rm e}^{{\rm i}(\omega-\omega_{eg})t - {\rm i}\omega_0(n-m)t - \gamma t}, \quad (1)$$

where the line-broadening parameter γ is introduced phenomenologically. F_{mn} is the Franck-Condon wavefunction overlap integral for the m to n transition

$$F_{mn} = \langle m| \exp\left(-\frac{d}{\sqrt{2}}\left(\hat{a}^\dagger - \hat{a}\right)\right)|n\rangle \quad (2)$$

given in terms of bosonic (vibrational) creation $\hat{a}^\dagger$ and annihilation $\hat{a}$ operators[29,30].

B. Molecule coupled to the phonon bath

In order to capture both the vibrational-type set of states of the energy spectrum and the spectral broadening in an unified model a more general description of a molecule is needed. The model discussed above considered the composite electronic+vibrational system as a closed system. Consequentially, the line-broadening parameter γ was included phenomenologically and without more detailed physical insight.

The total Hamiltonian of a single molecule coupled to the set of phonon modes (an open quantum system) is given by

$$\begin{aligned}\hat{H} = 0|g\rangle\langle g| + (\omega_{eg}+\lambda)|e\rangle\langle e| \\ -\sum_\alpha \hbar\omega_0^{(\alpha)}\sqrt{s_\alpha}\left(\hat{a}_\alpha^\dagger + \hat{a}_\alpha\right)|e\rangle\langle e| \\ +\sum_\alpha \hbar\omega_0^{(\alpha)}\left(\hat{a}_\alpha^\dagger\hat{a}_\alpha + \frac{1}{2}\right).\end{aligned} \tag{3}$$

Here the ground state $|g\rangle$ is the reference zero-energy state, the energy of the excited state $|e\rangle$ is additionally shifted by the reorganization energy $\lambda = \sum_\alpha \hbar\omega_0^{(\alpha)} s_\alpha$, while the rest of vibrational degrees of freedom are represented by a set $\{\alpha\}$ of harmonic oscillators. The system-bath coupling represented by the third term in Eq. (3) introduces fluctuations into the energy of the electronic excited state due to low-frequency bath modes at fixed temperature. The most convenient form to describe such fluctuations is the time correlation function:

$$C(t) = \mathrm{Tr_B}\left\{Q_\mathrm{e}(t)Q_\mathrm{e}(0)\rho_\mathrm{eq}\right\}. \tag{4}$$

Here

$$\rho_\mathrm{eq} = \mathcal{Z}^{-1}\exp\left(-\sum_\alpha \beta\hbar\omega_0^{(\alpha)}\left(\hat{a}_\alpha^\dagger\hat{a}_\alpha + \frac{1}{2}\right)\right) \tag{5}$$

is the normalized thermally equilibrated canonical density operator of the bath ($\beta^{-1} = k_\mathrm{B}T$), and

$$Q_\mathrm{e}(t) = \sum_\alpha \hbar\omega_0^{(\alpha)}\sqrt{s_\alpha}\left(\hat{a}_\alpha^\dagger(t) + \hat{a}_\alpha(t)\right) \tag{6}$$

is the fluctuating collective bath coordinate in the Heisenberg representation. The exact form of the correlation function describes the high-frequency modes as well. Trace in Eq. (4) amounts to averaging over the infinite set $\{\alpha\}$ of harmonic oscillators. Inclusion of eqs. (5) and (6) into the trace gives

$$C(t) = \sum_\alpha \hbar^2\left(\omega_0^{(\alpha)}\right)^2 s_\alpha\left(\coth\frac{\beta\hbar\omega_0^{(\alpha)}}{2}\cos\omega_0^{(\alpha)}t - \mathrm{i}\sin\omega_0^{(\alpha)}t\right) \tag{7}$$

which is the well-known form of the two-point correlation function of generalized bath coordinates[30]. The Fourier transform of the correlation function is a real function

$$\mathcal{C}(\omega) = \int_{-\infty}^{\infty}\mathrm{d}t\mathrm{e}^{\mathrm{i}\omega t}C(t) \equiv \mathcal{C}'(\omega) + \mathcal{C}''(\omega), \tag{8}$$

where $\mathcal{C}'(\omega)$ and $\mathcal{C}''(\omega)$ are even and odd functions of ω. $\mathcal{C}''(\omega)$ is the temperature-independent function and is denoted as the spectral density:

$$\mathcal{C}''(\omega) = -2\int_0^\infty \sin\omega t\mathrm{Im}C(t)\mathrm{d}t. \tag{9}$$

$\mathcal{C}'(\omega)$ and $\mathcal{C}''(\omega)$ are related by the fluctuation-dissipation theorem

$$\mathcal{C}'(\omega) = \coth\left(\beta\hbar\omega/2\right)\mathcal{C}''(\omega). \tag{10}$$

To describe the optical properties of the molecule the system polarization operator $\hat{P} = |g\rangle\langle e| + |e\rangle\langle g|$ is assumed (the transition dipole strength is taken as unity). It can be shown that the quantum correlation functions of the polarization operator representing the spectroscopic observables are exactly given in terms of the second-order cumulant expansion with respect to the vibrational modes[30]. Therefore, it is exact for our molecule and we can calculate the shapes of electronic transition bands and the bath-induced time dependence of the spectrum by using the formalism of the lineshape functions. The latter directly comes from the perturbative second-order cumulant expansion of the system density operator propagation which allows to describe various types of vibrational baths and include these effects explicitly[31]. The absorption coefficient is then given by

$$\kappa_\mathrm{abs}^{\mathcal{C}}(\omega) \propto \omega\mathrm{Re}\int_0^\infty \mathrm{d}t\mathrm{e}^{\mathrm{i}(\omega-\omega_0)t - g(t)}. \tag{11}$$

Here dimensionless lineshape function $g(t)$ is an integral transformation of the correlation function $C(t)$ of system-bath fluctuations, or for its Fourier transform (Eq. (8)),

$$g(t) \equiv -\frac{1}{2\pi}\int_{-\infty}^{\infty}\mathrm{d}\omega\frac{\mathcal{C}(\omega)}{\omega^2}\left[\exp(-\mathrm{i}\omega t) + \mathrm{i}\omega t - 1\right]. \tag{12}$$

Assuming that the system is coupled to a continuous spectrum of bath frequencies, the correlation function Eq. (7) can be calculated for a predefined distribution. We introduce the density of the Huang-Rhys parameter as a function of vibronic frequency, $\{s_\alpha\} \to s(\omega)\mathrm{d}\omega$, which may have a peak at some dominant normal-mode frequency ω_0. Then, from eqs. (7) and (9) the spectral density is obtained as

$$\mathcal{C}''(\omega) = \pi\hbar^2\omega^2\left[s(\omega) - s(-\omega)\right]. \tag{13}$$

For instance, if we consider a vibrational damped mode it will be represented by a broad peak in the spectral density of the system-bath coupling. In case of the Gaussian-type coupling

$$s_\mathrm{G}(\omega) = \frac{1}{\sqrt{2\pi}\gamma}\mathrm{e}^{-\frac{(\omega-\omega_0)^2}{2\gamma^2}} \tag{14}$$

the spectral density function is

$$\mathcal{C}''_\mathrm{G}(\omega) = \lambda\mu\cdot\frac{\sqrt{\pi}}{\sqrt{2}\gamma}\left[\mathrm{e}^{-\frac{(\omega-\omega_0)^2}{2\gamma^2}} - \mathrm{e}^{-\frac{(\omega+\omega_0)^2}{2\gamma^2}}\right], \tag{15}$$

while the Lorentzian-type coupling

$$s_\mathrm{L}(\omega) = \frac{1}{\pi}\frac{1}{(\omega-\omega_0)^2+\gamma^2} \tag{16}$$

leads to

$$\mathcal{C}''_{\rm L}(\omega) = \lambda\mu \cdot \frac{4\omega\omega_0\gamma}{\left(\omega^2-\omega_0^2-\gamma^2\right)^2+4\omega^2\gamma^2}. \qquad (17)$$

Here λ and μ are just some scaling constants here inserted for convenience: the expression of μ is later chosen in order for λ to be equal to the reorganization energy $\pi^{-1}\int_0^\infty \frac{{\rm d}\omega}{\omega}\mathcal{C}''(\omega)$.

By this point, no approximations were applied – equations (15) and (17) are consistent with the fluctuation-dissipation theorem. The inverse Fourier transform of them would give the time correlation functions which in case of Gaussian and Lorentzian couplings decay as $\mathrm{e}^{-\gamma^2t^2/2}$ and $\mathrm{e}^{-\gamma t}$, respectively. The spectral densities include the damping parameter γ and vibrational frequency ω_0. By taking various limits with respect to these parameters, different damping regimes can be achieved representing different conditions of the bath and both spectral densities (eqs. (15) and (17)) can be used in numerical simulations.

We further analyze different regimes of undamped, damped and overdamped vibrational motion considering the Lorentzian-type coupling since it is related to the exponentially-decaying time correlation function, which is a natural decay pattern in most of physical applications. When a single bath mode is assumed, i. e. when the spectral density function is obtained as a Fourier transform of a single term of Eq. (7), the spectral density is given by

$$\mathcal{C}''_{\rm u}(\omega) = \pi s\omega_0^2\left[\delta(\omega-\omega_0)-\delta(\omega+\omega_0)\right]. \qquad (18)$$

The reorganization energy in this case is $s\omega_0$ and the lineshape function is

$$g_{\rm u}(t) = s\left[\coth\frac{\beta\hbar\omega_0}{2}\left(1-\cos\omega_0 t\right)+{\rm i}\left(\sin\omega_0 t-\omega_0 t\right)\right]. \qquad (19)$$

This vibrational mode leads to non-decaying, undamped, vibrational motion. Such spectral density given by the δ-functions is not realistic because dissipation, which accompanies any vibrational motion due to the molecular interaction with its environment, is neglected. Damping induces the decay of the correlation function over time and the corresponding spectral density should have a finite-width smooth peak. Such damped regime is achieved by taking $\gamma<\omega_0$ in Eq. (17) and leads to

$$\mathcal{C}''_{\rm d}(\omega) = \frac{2\sqrt{2}\lambda\omega\omega_0^2\gamma}{\left(\omega^2-\omega_0^2\right)^2+2\gamma^2\omega^2}. \qquad (20)$$

This spectral density function with reorganization energy λ has a peak at ω_0 and the peak width is defined by the damping strength γ, differently from Eq. (18), where the peak is the δ-function (Fig. 2a).

The opposite, overdamped, regime is usually represented by the spectral density of a Brownian oscillator, which represents the fluctuations of the Ornstein-Uhlenbeck process[32]. This regime can be postulated

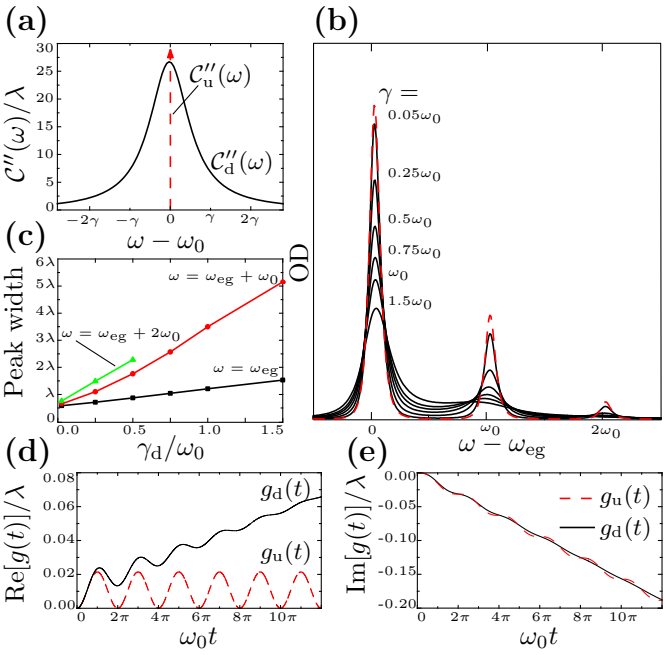

Fig. 2. (a) Spectral densities of undamped (red dashed line) and damped (black solid line) baths. (b) Absorption spectra of the displaced harmonic oscillator ($s=0.3$) for different damping strengths $\gamma/\omega_0 = 0.05-1.5$ of the damped bath (black solid lines) and for the undamped bath (red dashed line). The widths of three main peaks are displayed as the functions of damping strengths in (c), where the third peak becomes unresolvable for $\gamma > 0.5\omega_0$. The real and imaginary parts of the lineshape functions corresponding to the different vibrational bath models are plotted in (d) and (e), respectively.

semi-classically, i. e. by using the exponentially decaying classical correlation function $\mathcal{C}_{\rm cl}(t) = 2\lambda k_{\rm B}T\exp(-\gamma|t|)$. Its Fourier transform $\mathcal{C}_{\rm cl}(\omega) = 4\gamma\lambda k_{\rm B}T(\omega^2+\gamma^2)^{-1}$ now represents the even (classical) part $\mathcal{C}'(\omega)$ of the total quantum correlation function. Since the classical trajectory reflects the high temperature limit, we have $\mathcal{C}''(\omega) = \frac{1}{2}\beta\hbar\omega\mathcal{C}'(\omega)$ and obtain the spectral density representing the classical Brownian particle[30]

$$\mathcal{C}''_{\rm o-sc}(\omega) = \frac{2\lambda\gamma\omega}{\omega^2+\gamma^2} \qquad (21)$$

with reorganization energy λ and the relaxation rate γ. The full quantum correlation function in the frequency domain can now be constructed by the direct application of the fluctuation-dissipation relation Eq. (10). Therefore, we denote bath described by such spectral density as the overdamped semi-classical bath. At the high-temperature limit the corresponding lineshape function is obtained as

$$g_{\rm o-sc}(t) = \frac{\lambda}{\gamma}\left(\frac{2}{\beta\gamma}-{\rm i}\right)\left(\mathrm{e}^{-\gamma t}+\gamma t-1\right). \qquad (22)$$

Evidently, the overdamped bath can also be obtained from Eq. (17). In the limit of $\gamma \gg \omega_0$ it yields rather

different expression

$$\mathcal{C}''_{\mathrm{o-q}}(\omega) = \frac{4\lambda\omega\gamma^3}{(\omega^2+\gamma^2)^2}. \tag{23}$$

We denote this regime as the quantum overdamped. The reorganization energies are equal to λ for both types of the overdamped spectral density. The semi-classical spectral density function is equal to λ at its maximum at $\omega = \gamma$, while the quantum function has its maximum value $\mathcal{C}''_{\mathrm{o-q}}(\omega_{\mathrm{peak}}) = \frac{3\sqrt{3}}{4}\lambda \approx 1.3\lambda$, where $\omega_{\mathrm{peak}} = \sqrt{3}/3\gamma \approx 0.58\gamma$ (see Fig. 3a). The quantum overdamped spectral density decays faster at infinity, therefore, it is more suitable for numerical applications. At the high-temperature limit the corresponding lineshape function is given by

$$\begin{aligned} g_{\mathrm{o-q}}(t) = \frac{\lambda}{\gamma}\left(\frac{2}{\beta\gamma} - \mathrm{i}\right)\left(\mathrm{e}^{-\gamma t}\gamma t + 2\mathrm{e}^{-\gamma t} - 2 + \gamma t\right) \\ + \frac{\lambda\beta}{2}\left(1 + \frac{4}{\beta^2\gamma^2}\right)\left(\mathrm{e}^{-\gamma t} + \gamma t - 1\right). \end{aligned} \tag{24}$$

III. SPECTROSCOPIC OBSERVABLES

The absorption signals of the two-level system coupled to the bath are calculated according to Eq. (11) and using lineshape functions corresponding to different damping regimes (eqs. (18), (20), (21) or (23)). The included overdamped modes lead to the Lorentzian or Gaussian lineshapes of spectral peaks for fast, $2\lambda\beta^{-1}\gamma^{-2} \gg 1$, or slow, $2\lambda\beta^{-1}\gamma^{-2} \ll 1$, decay regimes, respectively. Fast-decaying modes of molecular vibrations will result in homogeneous broadening, while the strong coupling to the high-frequency vibrations will result in vibrational progression in the absorption spectrum.

In the case when the molecule is coupled to a single high-frequency mode and a continuum of low-frequency damping modes the spectral density consists of two parts:

$$\mathcal{C}''(\omega) = \mathcal{C}''_{\mathrm{o}}(\omega) + \mathcal{C}''_{\mathrm{vib}}(\omega). \tag{25}$$

Here the (fast) $\mathcal{C}''_{\mathrm{o}}(\omega)$ mode corresponds to the semi-classical $\mathcal{C}''_{\mathrm{o-sc}}(\omega)$ or quantum $\mathcal{C}''_{\mathrm{o-q}}(\omega)$ overdamped bath. The second term, $\mathcal{C}''_{\mathrm{vib}}(\omega)$, represents spectral density of (slow) molecular vibrations (undamped $\mathcal{C}''_{\mathrm{u}}(\omega)$ or damped $\mathcal{C}''_{\mathrm{d}}(\omega)$). The total lineshape function, which is a linear transformation of the spectral density, then contains two parts as well.

The spectral density and lineshape function formalism presented above is extended to the photon echo signal calculations for the 2D ES[33]. The response function theory denotes the response function $S(t_3, t_2, t_1)$ as a sum of different pathways of system density operator propagations. In this study we assume the impulsive limit (laser pulses of infinitesimally short duration), where the 2D spectrum is defined by the two-dimensional Fourier transform of the response function over variables t_1 and t_3; these then have the meanings of the time delays between the first and the second laser pulses, and the third laser pulse and the detection time, respectively[34]. t_2 is the fixed time delay between the second and the third interaction and is denoted as the population time. The rephasing $\boldsymbol{k}_{\mathrm{I}}$ (Fig. 4) and nonrephasing $\boldsymbol{k}_{\mathrm{II}}$ (Fig. 5) signals are distinguished as the ordering of the interaction with the first two pulses is changed. The total signal is denoted as the sum of $\boldsymbol{k}_{\mathrm{I}}$ and $\boldsymbol{k}_{\mathrm{II}}$ parts. Evolution of its diagonal and off-diagonal peaks closely follows the dynamics of corresponding populations and quantum coherences of the system density operator. In 2D spectra, fast-decaying modes of molecular vibrations will result in anti-diagonal peak (homogeneous) broadening, while the strong coupling to the high-frequency vibrations will result in multiple oscillating diagonal and off-diagonal peaks reflecting the configuration of vibrational states[35,36].

For a single two-level system the complete expressions for the rephasing and nonrephasing contributions of 2D spectrum can be given in terms of the lineshape functions:

$$\begin{aligned} S_{\boldsymbol{k}_{\mathrm{I}}}(t_3,t_2,t_1) = \frac{1}{2}\mathrm{e}^{-\mathrm{i}\omega_0(t_3-t_1)} \\ \times \mathrm{e}^{-g^*(t_1+t_2)-g^*(t_1)+g^*(t_1+t_2+t_3)} \\ \times \mathrm{e}^{\mathrm{Re}[g(t_2+t_3)+g(t_2)-g(t_3)]} \\ \times \cos\left\{\mathrm{Im}\left[g(t_2+t_3)+g(t_2)+g(t_3)\right]\right\} \end{aligned} \tag{26}$$

and

$$\begin{aligned} S_{\boldsymbol{k}_{\mathrm{II}}}(t_3,t_2,t_1) = \frac{1}{2}\mathrm{e}^{-\mathrm{i}\omega_0(t_3+t_1)} \\ \times \mathrm{e}^{g(t_1+t_2)-g(t_1)-g(t_1+t_2+t_3)} \\ \times \mathrm{e}^{\mathrm{Re}[g(t_2+t_3)+g(t_2)-g(t_3)]} \\ \times \cos\left\{\mathrm{Im}\left[g(t_2+t_3)+g(t_2)-g(t_3)\right]\right\}, \end{aligned} \tag{27}$$

respectively. It should be noted that these expressions are exact for the harmonic bath and carry no approximation[31].

For a multi-chromophoric system the response function is a sum of many contributions, which can be classified to the excited state absorption, excited state emission and ground state bleaching pathways. Additionally, the pathways responsible for population transfer are present[35]. Here in eqs. (26) and (27), there are only two pathways; the excited state absorption contribution producing negative peaks in the 2D spectrum is not available due to absence of the third electronic state.

A. Quantum vs. semi-classical overdamped bath

The differences in the two-level system absorption lineshapes obtained by using solely the quantum or semi-classical overdamped bath models ($\mathcal{C}''(\omega) \equiv \mathcal{C}''_{\mathrm{o}}(\omega)$) are minor (Fig. 3b) despite of a substantial difference in the shapes of spectral densities (Fig. 3a). The position of the absorption spectra are mainly determined by the

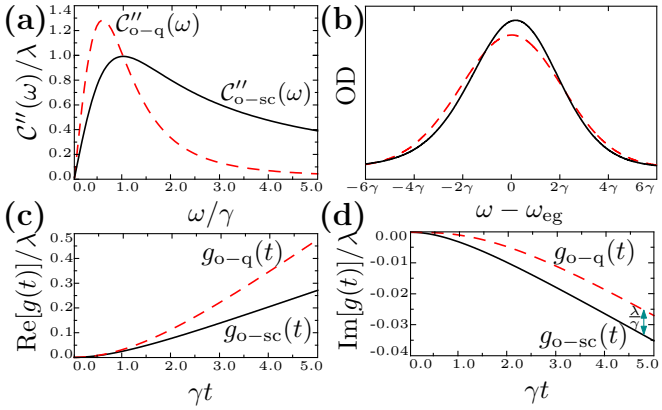

Fig. 3. (a) Overdamped quantum (red dashed line) and semi-classical (black continuous line) spectral density functions of an two-level system and corresponding (b) absorption spectra, (c-d) real and imaginary parts of the lineshape functions.

imaginary part of the corresponding lineshape function (Fig. 3d): for the semi-classical bath, it is lower by λ/γ compared to the quantum bath at $\gamma t \gg 1$. The slopes of the imaginary parts are, however, both equal. The slopes of the real parts of the lineshape functions, which determine the absorption linewidth, are different (Fig. 3c). For $g_{\mathrm{o-sc}}(t)$ the function slope at $\gamma t \gg 1$ is $\frac{2\lambda}{\beta\gamma}$, while for $g_{\mathrm{o-q}}(t)$ is at least twice larger, $\frac{4\lambda}{\beta\gamma}+\frac{\lambda\beta\gamma}{2}$. Such differences result in larger lineshape broadening in the case of the quantum bath.

The shapes of functions describing the spectral peak dynamics of the rephasing 2D spectra obtained by using the quantum model of the overdamped bath (Eq. (24)) coincide with the semi-classical bath simulations (Eq. (22)) at short population times, as demonstrated in Fig. 4b and Fig. 4d. However, in the non-rephasing (Fig. 5b and Fig. 5d) spectrum the quantum overdamped bath changes both the amplitudes of oscillations and the averages of peak intensities. In the 2D spectra the quantum overdamped bath model produces lineshapes with slightly smaller broadening. By adjusting the parameters both models can be tuned to reflect experimental broadenings. The quantum model has a short tail in the spectral density, which is advantageous for numerical simulations.

B. Undamped vs. damped harmonic bath

The properties of undamped and damped harmonic baths are demonstrated by assuming the composite spectral density given by Eq. (25) and setting the Huang-Rhys factor of the coherent mode to $s = 0.3$. In absorption, such system demonstrates three well-resolved peaks of vibrational progression at frequencies $\omega = \omega_{\mathrm{eg}}, \omega_{\mathrm{eg}}+\omega_0$ and $\omega_{\mathrm{eg}} + 2\omega_0$ (Fig. 2b).

The case when the composite spectral density is $\mathcal{C}''_{\mathrm{o-sc}}(\omega) + \mathcal{C}''_{\mathrm{u}}(\omega)$ corresponds to the overdamped semi-classical bath with undamped vibrations. This is the commonly used approach and is discussed in detail in the literature[4,19,37]. The produced vibrational progression in the absorption spectrum is drawn as the red dashed line in Fig. 2b. Unsurprisingly, the absorption signal calculated from eqs. (1) and (11) are then identical.

The effects caused by damping of vibrations are often ignored, however they may raise significant implications in the nonlinear spectra. In the linear spectra, comparison of the result obtained by assuming the spectral density of $\mathcal{C}''_{\mathrm{o-sc}}(\omega) + \mathcal{C}''_{\mathrm{d}}(\omega)$ (black solid lines in Fig. 2b) to the undamped vibrations reveals an almost perfect correspondence for $\gamma = 0.05\omega_0$, which illustrates a smooth transition from one model to another. It is also noticeable that the peaks in the progression broaden gradually when the damping strength γ is increased. However, the broadening is not uniform – peaks that are at higher energies are broadened more. This is evident by evaluating peaks width dependence in the damping strength (Fig. 2c), obtained by fitting the spectra with multiple Lorentzian functions. As a result, the total spectral lineshape becomes asymmetric: higher-energy shoulder of the vibrational progression is reduced due to additional broadening. Such pattern of broadening is consistent with the lifetime-induced decay of vibrational coherences at higher excitation energies.

The peak lineshapes in the 2D spectra obtained by using the damped case show slightly larger broadenings compared to those of the undamped vibrations both for rephasing and nonrephasing signals (figs. 4 and 5). The non-uniform broadening, as follows from the absorption simulations, shows up in the 2D spectrum, as well. For the vibrational bath we separately study two cases: the damped vibrations ($\gamma = \omega_0/4$, Fig. 4a-b and Fig. 5a-b) and the undamped vibrations ($\gamma \to 0$, Fig. 4c-d and Fig. 5c-d). In both cases the lineshape function representing the semi-classical overdamped bath is added to the vibrational part. The reorganization energy in all cases is the same ($2s\omega_0$).

The vibrational wavepacket (coherence) beats show up as temporal oscillations in the 2D spectrum. Decay of the coherences in case of the damped vibrations results in decay of cross-peaks (compare spectra for $t_2 = 2\pi\omega_0^{-1}$ in Fig. 4a and Fig. 4c): since all spectra are normalized to the maximum of the rephasing signal at $t_2 = 0$, the intensities of the cross-peaks and the upper diagonal peak are evidently lower than those of the main peak at $(\omega_1, \omega_3) = (\omega_{\mathrm{eg}}, \omega_{\mathrm{eg}})$. The main differences in oscillatory dynamics of peaks in the 2D spectra are due to the damping-induced decay of coherences in the case of the damped vibrations.

Considering the phases of oscillations corresponding to different peaks, it is clearly observed that the model of vibrational bath does not change the phase relationships of peak oscillations. In general, the phases of peak oscillations are not the same for all peaks in rephasing and nonrephasing signals. For example, in the rephasing signal lower diagonal peak '$\mathrm{D_L}$' oscillates as the negative co-

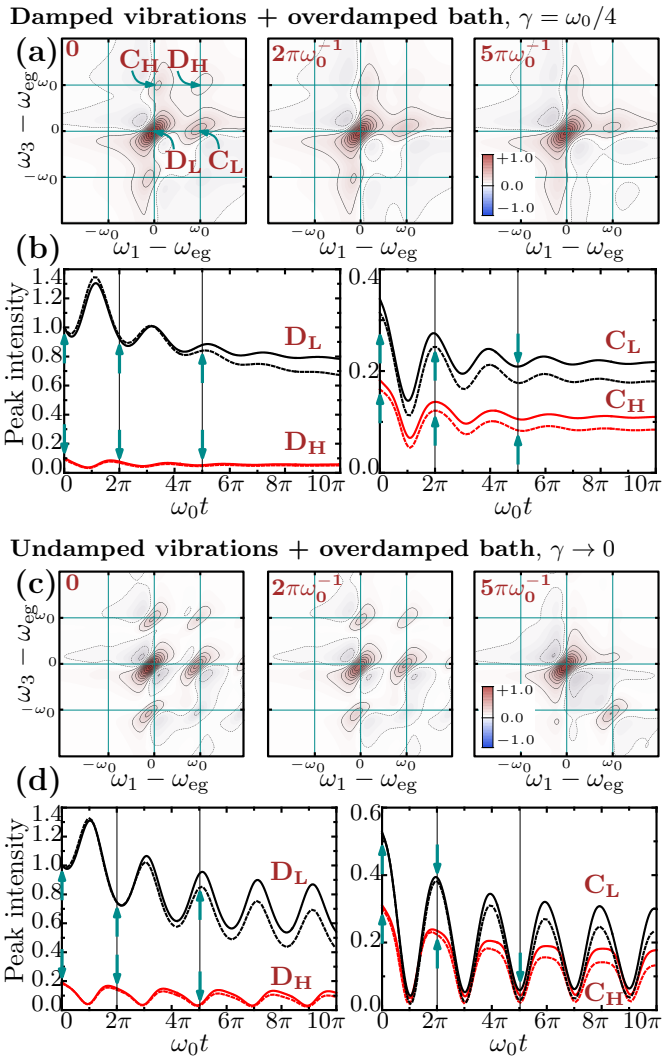

Fig. 4. 2D rephasing spectra at $t_2 = 0$, $2\pi\omega_0^{-1}$ and $5\pi\omega_0^{-1}$ with damped (a) and undamped (c) vibrations on top of the semi-classical bath. Intensities of the peaks, indicated by 'D_L' (diagonal lower), 'C_H' (cross-peak higher), etc., are depicted as functions of population time t_2 in case of damped vibrations (b) and undamped vibrations (d) with semi-classical (solid lines) and quantum (dashed lines) overdamped bath. All values are normalized to the maximum of the rephasing spectrum at $t_2 = 0$.

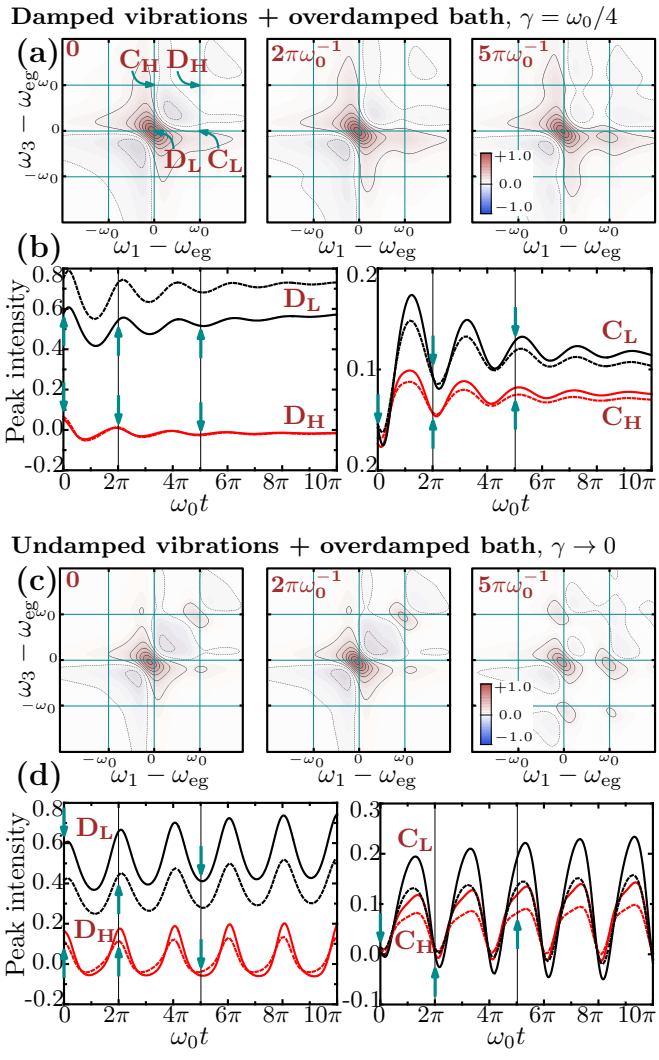

Fig. 5. 2D nonrephasing spectra at $t_2 = 0$, $2\pi\omega_0^{-1}$ and $5\pi\omega_0^{-1}$ with damped (a) and undamped (c) vibrations on top of the semi-classical bath; the intensities of corresponding peaks in case of damped vibrations (b) and undamped vibrations (d) with semi-classical (solid lines) and quantum (dashed lines) overdamped bath. All values are normalized to the maximum of the corresponding rephasing spectrum at $t_2 = 0$ (in Fig. 4).

sine function with the population time t_2, while all other peaks oscillate with opposite phase (Fig. 4b and Fig. 4d); in the nonrephasing signal (Fig. 5b and Fig. 5d) both cross-peaks oscillate as the negative cosine, while both diagonal peaks – with the opposite phase. Such phase relationships are typical for oscillations of vibrational coherences and are known as being strongly dependent on the Huang-Rhys factor; this property ought to be employed in distinguishing vibrational and electronic coherences in spectra[19].

IV. DISCUSSION

We considered the smooth transition from undamped through damped to overdamped vibrations and their possible manifestation in the 2D ES signals. For small values of damping parameters ($\gamma < \lambda$) the undamped vibrational model can be used, but for $\gamma \approx \lambda$, effects of non-uniform peak broadening in absorption and the damping strength-dependent decay of coherences in the 2D signal become significant. We also introduced the quantum overdamped spectral density model which has a convenient decay character with frequency and can be used to model broadening effects similar to the semi-classical model of overdamped Brownian motion.

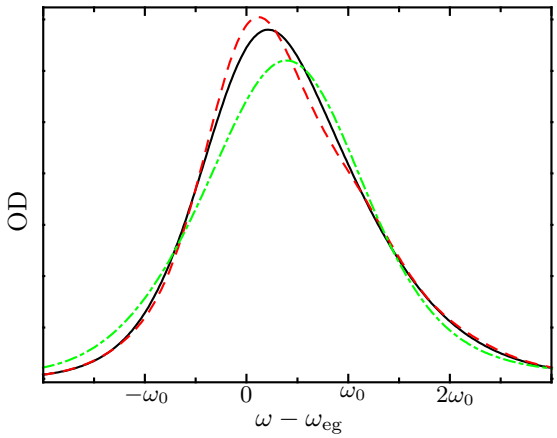

Fig. 6. Absorption spectra of the monomer with damped (solid black line) and undamped (dashed red line) vibrations; absorption spectrum of a dimer (green dash dotted line).

Understanding of the damping-related effects on the spectra is important when considering the realistic experimental measurements, where the mixture of electronic and vibrational quantum beats is expected to be observed.

To demonstrate the relations we turn to simulations and comparisons of model systems that have strong spectral congestion and underlying system properties may be obscure. To make a constructive parallel to the typical experimental results, properties of total spectra are highlighted rather than rephasing and nonrephasing spectra separately. We compare monomers coupled to (undamped and damped) vibronic resonances of frequency ω_0. The results are compared to the elementary molecular aggregate – a molecular homodimer with resonant coupling $|J| \equiv \frac{\omega_0}{2}$ (Fig. 6). The parameters of the monomer are the same as in Sec. III B. The 2D signals of the homodimer are simulated using the conventional response function theory for molecular excitons as described in Ref.[5]. The site energies of the dimer are taken to be $\varepsilon = \omega_{eg} + \frac{1}{2}\omega_0$ and the inter-dipole angle $\phi = \frac{2}{3}\pi$. Electronic transition to two excitonic states at ω_{eg} and $\omega_{eg} + \omega_0$ are then possible. The higher energy peak is more intensive than the lower one by factor $\frac{1-\cos\phi}{1+\cos\phi} = 3$. For such H-type dimer[38] the excited state absorption contribution will be much stronger in the lower cross-peak, making it negative in the 2D spectrum (Fig. 7a). The inter-dipole angle also determines the amplitudes of coherence oscillations. Reducing the angle would increase the amplitude of coherence oscillations, but decrease the excited state absorption influence on the lower cross-peak. The spectral density corresponding to the overdamped Brownian oscillator (overdamped semi-classical bath, Eq. (22)) is used for the spectral broadening. Its parameters are $\lambda = \frac{3}{5}\omega_0$ and $\gamma = \frac{1}{6}\omega_0$.

The total spectra of the monomer with undamped vibrations (Fig. 7b) show a typical non-decaying 'breathing' behavior of the main peak[16,17]. It can be characterized as the anticorrelation of diagonal and antidiagonal widths of the main peak. Such change of the peak shape is created by the superposition of $\boldsymbol{k}_{\rm I}$ and $\boldsymbol{k}_{\rm II}$ signals, which have phase-inverted dependence of the peak intensity on t_2, as can be seen in Fig. 7e and Fig. 7f. The same relation is observed in simulations of systems with well-resolved peaks as shown in Fig. 4 and Fig. 5.

As it was already mentioned, the phase relationships and oscillation amplitudes of the $\boldsymbol{k}_{\rm I}$ and $\boldsymbol{k}_{\rm II}$ signals are Huang-Rhys factor-dependent, therefore, both correlation and anticorrelation of the diagonal peak-width and intensity is possible for different systems[17]. However, the anticorrelation of the diagonal width and intensity of any peak in the 2D spectrum is not available for the electronic dimer[39]. As follows from our calculations of a two-level system the amplitude is higher for the $\boldsymbol{k}_{\rm I}$ signal and, therefore, the correlation of the diagonal width and intensity of the main peak is observed both for damped and undamped vibrations. Thus, spectral dynamics of the vibrational and electronic-only systems are very similar by this aspect.

The monomer with damped vibrations being analyzed here is an illustration of the transition from damped to overdamped vibrations. Due to damping, the main peak experiences only a few 'breaths' and the round shape is established at $t_2 > 2.5\pi\omega_0^{-1}$ at least (Fig. 7c). Increasing the damping strength would destroy all vibrational coherences and it would not be possible to spectrally distinguish it from a general two-level system coupled to an overdamped bath. However, for a molecular dimer one can expect it to demonstrate similar spectral characteristics compared to the monomer with damped vibrations. Indeed, this is true for the 2D spectra presented in Fig. 7a. Due to the excited state absorption, a negative region below the main peak appears for short population times. The oscillation pattern of the peak maximum (green dot-dashed line in Fig. 7d-f) closely resembles the dependence of the monomer with damped vibrations (black solid line), as well. The decay rates of the signals are very similar here, but the established values of peak intensities at long population times are different. This can be explained by the additional dephasing mechanisms (exciton transfer and lifetime decay) available for an excitonic system during t_2.

V. CONCLUSIONS

Consideration of high-frequency damped molecular vibrations instead of undamped is a more realistic description since it includes dephasing and dissipation that vibronic motion experiences in solvent. This correction induces non-uniform peak broadening, changes the position of peaks within the vibrational progression in the absorption and results in decay of coherences in the 2D spectrum. The significance of the effect depends on the width of the spectral density function around the resonance. Therefore, having the coherence decay rate and

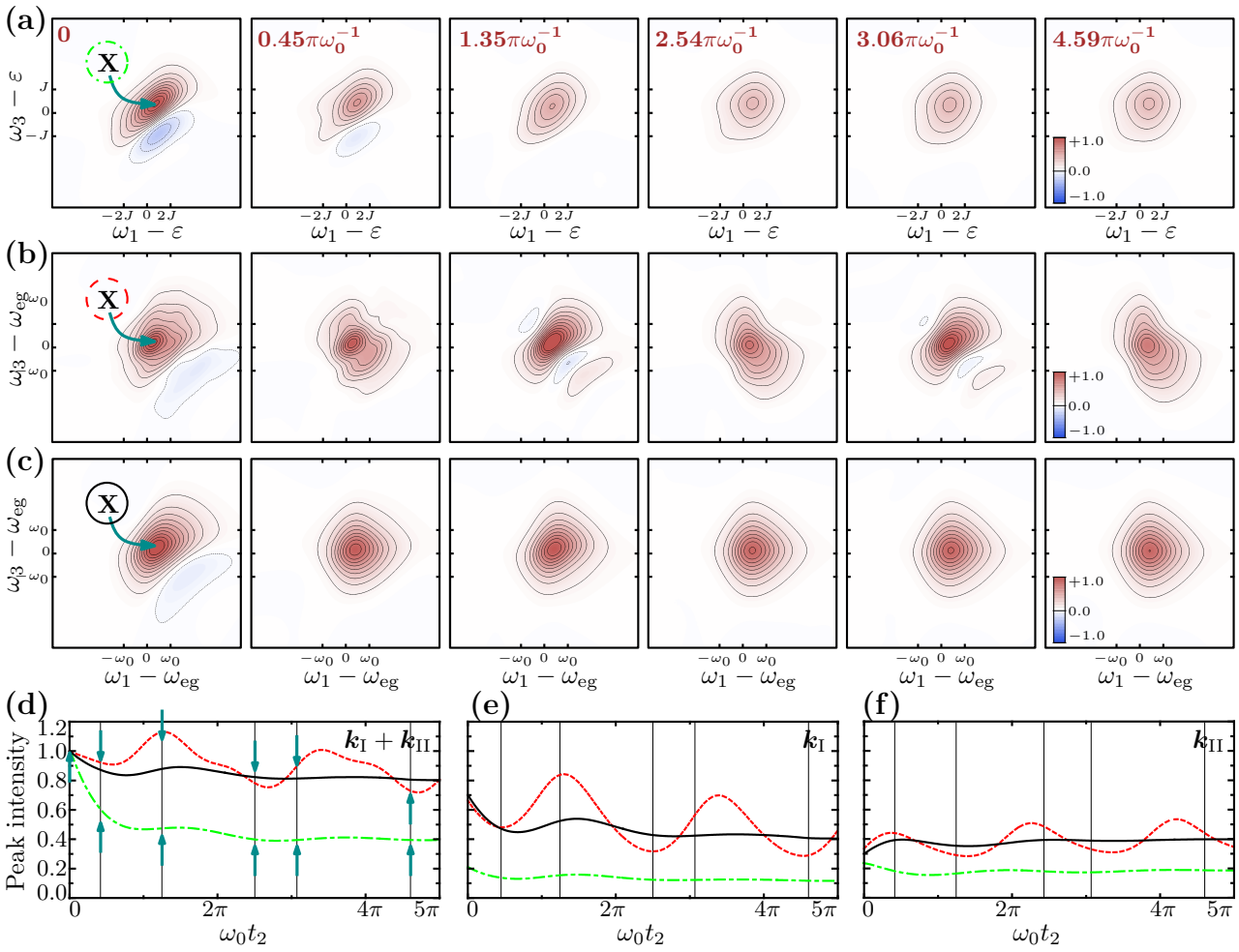

Fig. 7. Real parts of total ($\boldsymbol{k}_I + \boldsymbol{k}_{II}$) 2D spectra of a dimer (a) and a two-level system with undamped (b) and damped (c) vibrations at population times $t_2 = 0...4.59\pi\omega_0^{-1}$. Plots of intensities of peaks, indicated by 'X' of total (d), $\boldsymbol{k}_I$ (e) and $\boldsymbol{k}_{II}$ (f) signals of the monomer with damped vibrations (solid black lines), undamped vibrations (dashed red lines) and molecular dimer (dot dashed green lines) are depicted. Spectra are normalized to the values of intensity maxima at $t_2 = 0$ for each system separately.

the peak broadening quantitatively evaluated from the experiment, one would be able to estimate the damping parameters of vibrations.

A model of overdamped quantum bath is suggested in this paper. It is represented by the spectral density, which is directly obtained from the quantum-mechanical correlation function of bath coordinates and not assuming the classical correlation function as in the overdamped semi-classical bath model. The spectral density of the overdamped quantum bath decays as ω^{-3} at large frequencies, which is preferable to ω^{-1} used in overdamped semi-classical model. In two-dimensional photon echo signals, it results in increased homogeneous broadening of peaks. Dynamics of quantum beats is not affected by this spectral density; however, the ratio of rephasing and non-rephasing signals changes, as well as peak intensities.

Damping of vibrations causes the decay of coherences; its influence on the peak shape and correlation/anticorrelation of the diagonal peak width and intensity is reported to be insignificant compared to the description of undamped vibrations. Further increase of the damping strength results in instantaneous disappearance of vibrational coherences and this limit corresponds to purely overdamped vibrational motion.

ACKNOWLEDGMENTS

This research was partially funded by the European Social Fund under the Global grant measure.

REFERENCES

[1] Y. S. Kim and R. M. Hochstrasser, J. Phys. Chem. B **113**, 8231 (2009).

[2]P. F. Tian, D. Keusters, Y. Suzaki, and W. S. Warren, Science **300**, 1553 (2003).
[3]G. S. Engel, T. R. Calhoun, E. L. Read, T. K. Ahn, T. Mančal, Y. C. Cheng, R. E. Blankenship, and G. R. Fleming, Nature **446**, 782 (2007).
[4]T. Mančal, A. Nemeth, F. Milota, V. Lukeš, H. F. Kauffmann, and J. Sperling, J. Chem. Phys. **132**, 184515 (2010).
[5]D. Abramavicius, V. Butkus, J. Bujokas, and L. Valkunas, Chem. Phys. **372**, 22 (2010).
[6]H. Okamoto and K. Yoshihara, Chem. Phys. Lett. **177**, 568 (1991).
[7]Y.-C. Cheng and G. R. Flemig, J. Phys. Chem. A **112**, 4254 (2008).
[8]F. Perakis, S. Widmer, and P. Hamm, J. Chem. Phys **134**, 204505 (2011).
[9]E. Collini and G. D. Scholes, Science **323**, 5912 (2009).
[10]F. Caruso, A. W. Chin, A. Datta, S. F. Huelga, and M. Plenio, J. Chem. Phys. **131**, 105106 (2009).
[11]G. Panitchayangkoon, D. Hayes, K. A. Fransted, J. Caram, E. Harel, J. Wen, R. Blankenship, and G. Engel, Proc. Natl. Acad. Sci. USA **107**, 12766 (2010).
[12]E. L. Read, G. S. Engel, T. R. Calhoun, T. Mančal, T. K. Ahn, R. E. Blankenship, and G. R. Fleming, Proc. Nat. Acad. Sci. USA **104**, 14203 (2007).
[13]E. Collini, C. Y. Wong, K. E. Wilk, P. M. G. Curmi, P. Brumer, and G. D. Scholes, Nature **463**, 644 (2010).
[14]M. Bixon and J. Jortner, J. Chem. Phys. **107**, 1470 (1997).
[15]M. H. Vos, J. C. Lambry, S. J. Robles, D. C. Youvan, J. Breton, and J. L. Martin, **88**, 8885 (1991).
[16]A. Nemeth, F. Milota, T. Mančal, V. Lukeš, J. Hauer, H. F. Kauffmann, and J. Sperling, J. Chem. Phys. **132**, 184514 (2010).
[17]N. Christensson, F. Milota, J. Hauer, J. Sperling, O. Bixner, A. Nemeth, and H. F. Kauffmann, J. Phys. Chem. B **115**, 5383 (2011).
[18]D. B. Turner, K. E. Wilk, P. M. G. Curmi, and G. D. Scholes, J. Phys. Chem. Lett. **2**, 1904 (2011).
[19]V. Butkus, D. Zigmantas, L. Valkunas, and D. Abramavicius, ArXiv e-prints (2012), http://arxiv.org/abs/1201.2753.
[20]F. Caycedo-Soler, A. W. Chin, J. Almeida, S. F. Huelga, and M. B. Plenio, J. Chem. Phys **136**, 155102 (2012).
[21]T. Mančal, N. Christensson, V. Lukeš, F. Milota, O. Bixner, H. F. Kauffmann, and J. Hauer, J. Phys. Chem. Lett. **3**, 1497 (2012).
[22]N. Christensson, H. F. Kauffmann, T. Pullerits, and T. Mančal, J. Phys. Chem. B **0**, null (0).
[23]J. M. Womick and A. M. Moran, J. Phys. Chem. B **115**, 1347 (2011).
[24]T. Holstein, Ann. Phys. **8**, 325 (1959).
[25]Y.-C. Cheng and R. J. Silbey, J. Chem. Phys. **128**, 114713 (2008).
[26]J. Zhu, S. Kais, P. Rebentrost, and A. Aspuru-Guzik, J. Phys. Chem. B **115**, 1531 (2011).
[27]J. Hu, M. Luo, F. Jiang, R.-X. Xu, and Y. Yan, J. Chem. Phys **134**, 244106 (2011).
[28]J. Prior, A. W. Chin, S. F. Huelga, and M. B. Plenio, Phys. Rev. Lett. **105**, 050404 (2010).
[29]H. van Amerogen, L. Valkunas, and R. van Grondelle, Photosynthetic Excitons (World Scientific, Singapore, 2000).
[30]V. May and O. Kühn, Charge and Energy Transfer Dynamics in Molecular Systems (Wiley-VCH, Weinheim, 2011).
[31]S. Mukamel, Principles of Nonlinear Optical Spectrscopy (Oxford University Press, New York, 1995).
[32]H.-P. Breuer and F. Petruccione, The theory of open quantum systems (Oxford University Press, New York, 2002).
[33]D. Abramavicius, B. Palmieri, D. V. Voronine, F. Šanda, and S. Mukamel, Chem. Rev. **109**, 2350 (2009).
[34]V. Butkus, D. Abramavicius, A. Gelzinis, and L. Valkunas, Lith. J. Phys. **50**, 267 (2010).
[35]D. Abramavicius, L. Valkunas, and S. Mukamel, Europhys. Lett. **80**, 17005 (2007).
[36]V. Butkus, A. Gelzinis, and L. Valkunas, J. Phys. Chem. A **115**, 3876 (2011).
[37]D. Egorova, Chem. Phys. **347**, 166 (2008).
[38]A. Gelzinis, D. Abramavicius, and L. Valkunas, Phys. Rev. B **84**, 245430 (2011).
[39]A. V. Pisliakov, T. Mančal, and G. R. Fleming, J. Chem. Phys. **124**, 234505 (2006).